JOURNAL OF Materials CHEMISTRY

# Synthesis and characterization of processible conducting polyaniline/$V_2O_5$ nanocomposites

**Wu Chun-Guey,* Hwang Jiunn-Yih and Hsu Shui-Sheng**

*Department of Chemistry, National Central University, Chung-Li, Taiwan, 32054, Republic of China*

***Received 24th November 2000, Accepted 15th May 2001***
***First published as an Advance Article on the web 9th July 2001***

Flexible, conducting polyaniline/$V_2O_5$ nanocomposite films $(PAPSA)_xV_2O_5$ were prepared by simply mixing water soluble polyaniline, poly(aniline-*co*-*N*-(4-sulfophenyl)aniline) (PAPSA), with $V_2O_5$ at room temperature. Two types of $(PAPSA)_xV_2O_5$ films with different solubility were isolated. XRD data showed that the interlayer spacing of the water-soluble $(PAPSA)_xV_2O_5$ film, in which the polymer chains occupied the vacancies of $V_2O_5$ xerogel, is *ca.* $11.5 \pm 0.5$ Å. The *d*-spacing of the water insoluble $(PAPSA)_xV_2O_5$ film (small amount, $<5\%$) is $13.5 \pm 0.5$ Å, which is consistent with the insertion of polyaniline chains into the $V_2O_5$ interlayer space. In both phases, PAPSA and $V_2O_5$ were homogeneously mixed as revealed with SEM, depth profile SIMS and Auger analyses. The room-temperature conductivity of the water-soluble $(PAPSA)_xV_2O_5$ film was in between those of a PAPSA pellet and a $V_2O_5$ xerogel and the conductivity increased with temperature, characteristic of thermally activated behavior. Cyclic voltammograms of the nanocomposite films showed two pairs of red-ox peaks with good reversibility. The color of the films can be yellowish green, green, brown, orange or purple, depending on the applied potential and the stoichiometry of the composites. $(PAPSA)_xV_2O_5$ has much better electrochemical stability relative to PAPSA and its mechanical properties are superior to that of $V_2O_5$ xerogel.

## Introduction

Nature has been producing remarkable organic/inorganic composites, such as bone and nacre, for millions of years. Hybrid materials have also been used in industry for a long time, but the concept of hybrid organic–inorganic materials emerged only when research shifted to prepare more sophisticated materials with a higher added value.[1] At first glance, these materials are considered as biphase materials where the organic and inorganic phases are mixed at the μm or sub-μm scales. Nonetheless, it is obvious that the properties of these materials are not just the sum of the individual contributions from each of the phases, and tuning the properties of the materials is achieved by controlling the chemical nature of the interface interactions. Technological realizations for such advanced materials are expected in the field of 1D and 2D conductivity, membranes, anisotropic optical properties, and non-linear optics.[2] Several approaches to the production of such structures have been described, such as insertion of organic molecules or polymers in anisotropic inorganic networks.[3,4] Such frameworks could be either three-dimensional structures with large oriented tunnels[5] or two-dimensional structures with accessible interlayer spaces.[6] Using organic molecules or self-assembled aggregates as structure-directing agents, hybrid structures[7] and other forms,[8] can be assembled. Significant achievements have been accomplished in the last few decades.[9] The hybrid method is a creative strategy for obtaining new materials with novel properties.

Conducting polyaniline/$V_2O_5$ nanocomposites have been synthesized and well studied by Kanatzidis *et al.*[3] and others.[10] Such nanocomposites are prepared by *in situ* polymerization/intercalation of aniline in $V_2O_5$ xerogel. The resulting black films are insoluble and it is difficult to finely tune the stoichiometry of these nanocomposites. In this work, we report the synthesis of conducting water soluble polyaniline/$V_2O_5$ nanocomposites by simply mixing a poly(aniline-*co*-*N*-(4-sulfophenyl)aniline) (PAPSA) aqueous solution with $V_2O_5$ wet gel. The facile synthesis of conducting organic polymer/$V_2O_5$ nanocomposites with well-controlled stoichiometry is demonstrated and the structure, conductivity and spectroelectrochemical properties of these processible nanocomposites reported.

## Experimental section

### Materials

$(NH_4)_2S_2O_8$, $NaVO_3$, HCl(aq), *N*-(4-sulfophenyl)aniline and Dowex-50X2-100 resin were purchased from commercial resources and used as received. Aniline was dried over $CaH_2$ and freshly distilled before use.

### Preparation of water-soluble polyaniline, poly(aniline-*co*-*N*-(4-sulfophenyl)aniline)

Poly(aniline-*co*-*N*-(4-sulfophenyl)aniline) (PAPSA) was synthesized by reported methods[11] and was identified by IR and UV/Vis/NIR spectroscopy.

### Preparation of $V_2O_5$ xerogel

$V_2O_5$ xerogel was synthesized according to a literature report.[12] A $HVO_3$ solution was obtained by dissolving 4.0 g of $NaVO_3$ in 250 ml water, then passing the $NaVO_3$ aqueous solution through a $H^+$ ion exchange column packed with 30 g of Dowex-50X2-100 resin. Upon standing, the $HVO_3$ aqueous solution spontaneously polymerized to a red $V_2O_5$ gel *via* a sol–gel process. After evaporation of excess water, a dry gel (denoted xerogel) with a chemical formula of $V_2O_5 \cdot 1.6H_2O$ was obtained.

### Preparation of water-soluble polyaniline–$V_2O_5$ composites, $(PAPSA)_xV_2O_5$

In a typical reaction, known amounts of aqueous solution of water soluble poly(aniline-*co*-*N*-(4-sulfophenyl)aniline), PAPSA, was mixed well with the $V_2O_5$ wet gel. The mixture

DOI: 10.1039/b009419f

**Table 1** Polyaniline content, yield, room temperature conductivity, and solubility of poly(aniline-*co*-*N*-(4-sulfophenyl)aniline copolymers

| wt% of diphenylamine-4-sulfonate in the reactants | wt% of diphenylamine-4-sulfonate in the polymer | Yield (%) | Conductivity/S $cm^{-1}$ | Solubility |
|---|---|---|---|---|
| 83 | 70 | 33 | $5.0\times10^{-4}\sim1.0\times10^{-3}$ | Totally soluble |
| 70 | 68 | 47 | $5.0\times10^{-4}\sim1.0\times10^{-3}$ | Totally soluble |
| 63 | 70 | 60 | $5.0\times10^{-4}\sim1.0\times10^{-3}$ | Totally soluble |
| 55 | 65 | 62 | $5.0\times10^{-4}\sim5.0\times10^{-3}$ | Partially soluble |

was then centrifuged to separate the homogeneous suspension solution from the insoluble paste. The $(PAPSA)_xV_2O_5$ solution was casted on glass or silicon substrates. The excess water was evaporated, and a flexible conducting composite film, which can be peeled off as a freestanding film, was formed on the substrate. The colors of the films can be dark red, brown, or green, depending on the mole ratio of PAPSA and $V_2O_5$. The stoichiometry of the composites was determined by elemental analysis and TGA study. Since the insoluble portion is a relatively small amount ($<5\%$), studies were focused on the water-soluble portion.

### Physicochemical measurements

Fourier Transform infrared (FTIR) spectra were recorded for films on a Si substrate using a Bio-Rad 155 FTIR spectrometer. UV/Vis/NIR spectra were obtained using a Varian Cary 5E spectrophotometer in the laboratory atmosphere at room temperature. Scanning electron microscopy (SEM) and energy disperse spectroscopy (EDS) studies were done with Hitachi S-800 at 15 kV. X-Ray powder diffraction studies of the composite films were carried out with a Scintag Xgen-4000 X-ray diffractometer using Cu-K$\alpha$ radiation at 45 kV and 40 mA. Thermogravimetric analysis (TGA) was performed with a Perkin Elmer TGA-7 thermal analysis system using dry nitrogen (or oxygen) as a carrier gas at a flow rate of 100 ml $min^{-1}$. The TGA experiments were conducted from room temperature to 900 °C with a linear heating rate of 5 °C $min^{-1}$. X-Ray photoelectron spectroscopy studies were carried out on a Perkin-Elmer PHI-590AM ESCA/XPS spectrometer system with a cylindrical mirror electron (CMA) energy analyzer. The X-ray sources were Al K$\alpha$ at 600 W. and Mg K$\alpha$ at 400 W. Argon ion sputtering was performed using an Ar-ion gun at 4 kV beam energy and 25 mA emission current for 180 s intervals. Samples for the XPS studies were made as films on the substrates. The spectrum of gold was taken as a calibration standard before and after finishing the measurements. A Heraeus CHN-O-S Rapid-F002 system was used for elemental analysis of C, H, and N.

### Electrochemical studies

For the electrochemical measurements, composite films (*ca.* 2000 nm) were deposited on home-made ITO electrodes to construct a working electrode. Electrochemistry was performed in single-compartment, three-electrode cell with a Pt coil counter electrode and an Ag/AgCl reference electrode. The supporting electrolyte was 0.1 M $LiClO_4$ in acetonitrile. Cyclic voltammograms were recorded using a Model 263 electrochemical instrument (EG&G PAR) potentiostat/galvanostat with a scan rate of 100 mV $s^{-1}$. The color change of the composites under various applied potentials can be observed directly.

### Charge transport measurements

The electrical resistance as a function of temperature was measured using the constant-voltage, two-probe method with an applied voltage of 0.1 V. Silver paste was applied to make the electrical contacts. A Keithley 6512 programmable electrometer was used to provide the constant voltage source and measure the resulting current.

## Results and discussion

### A. Synthesis and characterization

**1. Preparation of poly(aniline-*co*-*N*-(4-sulfophenyl)aniline) (PAPSA).** The copolymer, PAPSA, was prepared by oxidizing mixtures containing different amounts of aniline and 4-sulfophenylaniline. The mole ratio of aniline and 4-sulfophenylaniline in the copolymer backbone (determined by elemental analysis and acid–base titration), the yield, the solubility and the conductivity of the copolymers are listed in Table 1. It was found that a high mole ratio of 4-sulfophenylaniline in the reacting mixture results in a low yield of the copolymer. This may be due to that pure poly-4-sulfophenylaniline was produced in the polymerization process but it was lost during product isolation. When the weight percentage of aniline to 4-sulfophenylaniline was higher than 60%, water insoluble copolymer also formed in the product. The copolymer prepared from the mixing of 37% of aniline with 63% of 4-sulfophenylaniline was used for the preparation of PAPSA–$V_2O_5$ composites. It is evident from Table 1 that the weight percentages of 4-sulfophenylaniline in the totally soluble copolymer backbone is close to 70% and did not change with alteration of the mole ratio of 4-sulfophenylaniline in the reactants, indicating that this material is most likely a regular copolymer. The $^1H$ NMR (300 MHz, $D_2O$) spectrum of copoly(aniline-4-sulfophenylaniline), Fig. 1, showed six doublets at chemical shifts between 7 and 8 ppm, corresponding to six types of aromatic hydrogen. The NMR data also indicated that the monomers in the copolymer backbone were arranged in a regular way.

**2. Synthesis of $(PAPSA)_xV_2O_5$ nanocomposites.** When an aqueous solution of PAPSA was mixed with $V_2O_5$ wet gel, a suspension in solution was formed, with no observable precipitate. To ensure the purity of the composite, the suspension solution was centrifuged to remove the insoluble paste. The clear solution and insoluble paste were then casted on a glass substrate; the excess water evaporated and dry films

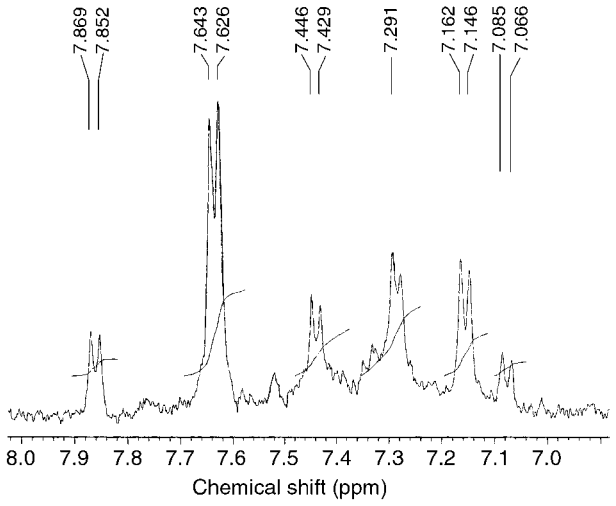


**Fig. 1** $^1H$ NMR ($D_2O$) spectrum of the copoly(aniline-4-sulfophenylaniline).

**Table 2** Solubilities, average interlayer spacings and domain sizes of $(PAPSA)_xV_2O_5$ samples

| Sample | Water solubility | *d*-Spacing[a]/Å | Domain size/Å |
|---|---|---|---|
| $V_2O_5$ xerogel | Soluble | 13.8 | 64 |
| $(PAPSA)_{0.05}V_2O_5$ | Soluble | 13.2 | 55 |
| $(PAPSA)_{0.1}V_2O_5$ | Soluble | 11.6 | 55 |
| $PAPSA)_{0.4}V_2O_5$ | Soluble | 11.3 | 50 |
| $PAPSA)_{1.2}V_2O_5$ | Soluble | 12.5 | 30 |
| $(PAPSA)_{0.1}V_2O_5$ | Insoluble | 14.1 | 76 |
| $(PAPSA)_{0.4}V_2O_5$ | Insoluble | 14.0 | 46 |
| $(PAPSA)_{0.8}V_2O_5$ | Insoluble | 13.3 | 50 |
| $(PAPSA)_{1.4}V_2O_5$ | Insoluble | 13.3 | 42 |

[a]The average of two measurements.

were obtained. The stoichiometries of the water soluble and insoluble composites obtained from elemental analysis and/or thermogravimetric analysis are listed in Table 2. It was found that the solubility is independent of the stoichiometry of the composites. This result suggested that there are two different arrangements of polyaniline chains in the $V_2O_5$ host. The *d*-spacing of $(PAPSA)_xV_2O_5$ calculated from X-ray diffraction patterns are also independent of the value of $x$. The interlayer spacing of the soluble fraction is $11.5 \pm 0.5$ Å, which is similar to $V_2O_5$ xerogel with a monolayer of $H_2O$ in its layer gallery. In contrast, the *d*-spacing of the insoluble composites with $x < 0.8$ are all close to 14.0 Å, similar to $PANI/V_2O_5$ prepared by *in situ* intercalation/polymerization of aniline in $V_2O_5$ xerogel.[3] The stoichiometries, interlayer spacing, and domain size of $(PAPSA)_xV_2O_5$ with various $x$ are also listed in Table 2. Depth profile SIMS, Fig. 2, and Auger analyses showed that the atomic ratios of N (or S) and V were very similar through the whole film. This indicated that the mixing between PAPSA and $V_2O_5$ was at the nanoscale level, therefore, $(PAPSA)_xV_2O_5$ can be viewed as a nanocomposite. When $x$ is higher than 1.5, the composites become amorphous, suggesting exfoliation of the $V_2O_5$ xerogel. The physicochemical properties of the water soluble $(PAPSA)_xV_2O_5$ are different from those of water insoluble $(PAPSA)_xV_2O_5$. The remainder of the paper will focus only on the water-soluble $(PAPSA)_xV_2O_5$ and differences between these two phases will be reported elsewhere.

**3. Physicochemical properties of water-soluble $(PAPSA)_x$-$V_2O_5$ nanocomposites.** IR spectra of water-soluble $(PAPSA)_x$-$V_2O_5$ films are shown in Fig. 3. All composites have three strong peaks at 1012, 751 and 570 $cm^{-1}$, which are the framework vibrations of $V_2O_5$, indicating that the framework of $V_2O_5$ remained intact when the composite was formed. The absorption peaks at 1590, 1483, 1167, and 1017 $cm^{-1}$, which belong to PAPSA, also did not change obviously. Nevertheless, the absorption at 1325 $cm^{-1}$ (C–N stretching of PAPSA) shifted to higher wavenumber. The shift of the C–N stretching peak to higher energy suggested that PAPSA was partially oxidized by $V_2O_5$. In order to investigate whether the polymer was oxidized by $V_2O_5$ or not, IR spectra were taken after PAPSA was treated with $(NH_4)_2S_2O_8$/HCl solution or electrochemically oxidized. The IR spectrum of oxidized PAPSA has a C–N stretching close that of PAPSA in the $(PAPSA)_xV_2O_5$ composite. Therefore, the interaction between PAPSA and $V_2O_5$ appears to be red-ox in nature. Thermogravimetric analysis of the composite and its individual components, Fig. 4, showed that the thermal stability of the PAPSA in $(PAPSA)_xV_2O_5$ is superior to that of the free polymer. The TGA data suggested that PAPSA chains are intercalated in a thermally stable host. An SEM micrograph (Fig. 5c) of the $(PAPSA)_{0.1}V_2O_5$ film revealed a homogeneous morphology with no phase separation observed. The surface morphology is smoother than those of PAPSA and $V_2O_5 \cdot 1.6H_2O$ xerogel films.

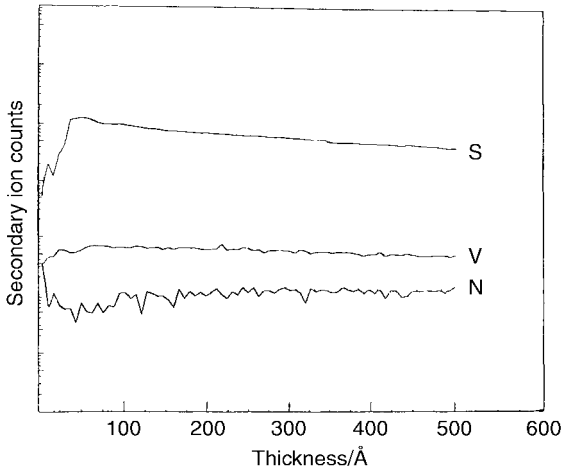


**Fig. 2** Depth profile secondary ion mass spectrometry (SIMS) analysis of $(PAPSA)_{0.1}V_2O_5$.

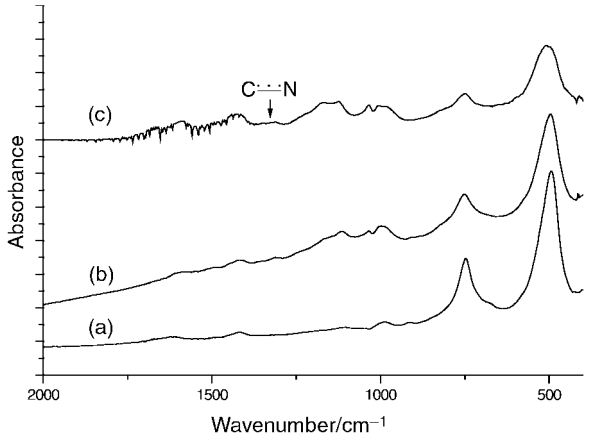


**Fig. 3** Infared spectra of water soluble films: (a) $(PAPSA)_{0.05}V_2O_5$, (b) $(PAPSA)_{0.37}V_2O_5$ and (c) $(PAPSA)_{1.18}V_2O_5$.

## B Charge transport and electrochemical properties of $(PAPSA)_xV_2O_5$ nanocomposites

PAPSA and $V_2O_5$ xerogel are both electrically conducting materials. The major charge carriers of these nanocomposites could be either polarons associated with $d^1$ ($V^{4+}$) centers found on the $V_2O_5$ lattice or bipolarons located on the PAPSA backbone. Therefore, the charge transport properties of $(PAPSA)_xV_2O_5$ will depend on the mobility of these two types of carriers. The variable-temperature conductance of $(PAPSA)_xV_2O_5$ is shown in Fig. 6d. The conductance increases

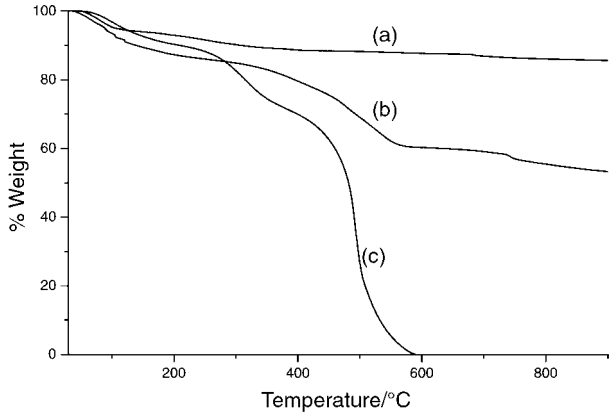


**Fig. 4** Thermogravimetric analysis (under oxygen) of (a) PAPSA, (b) $V_2O_5$ and (c) $(PAPSA)_{0.37}V_2O_5$.

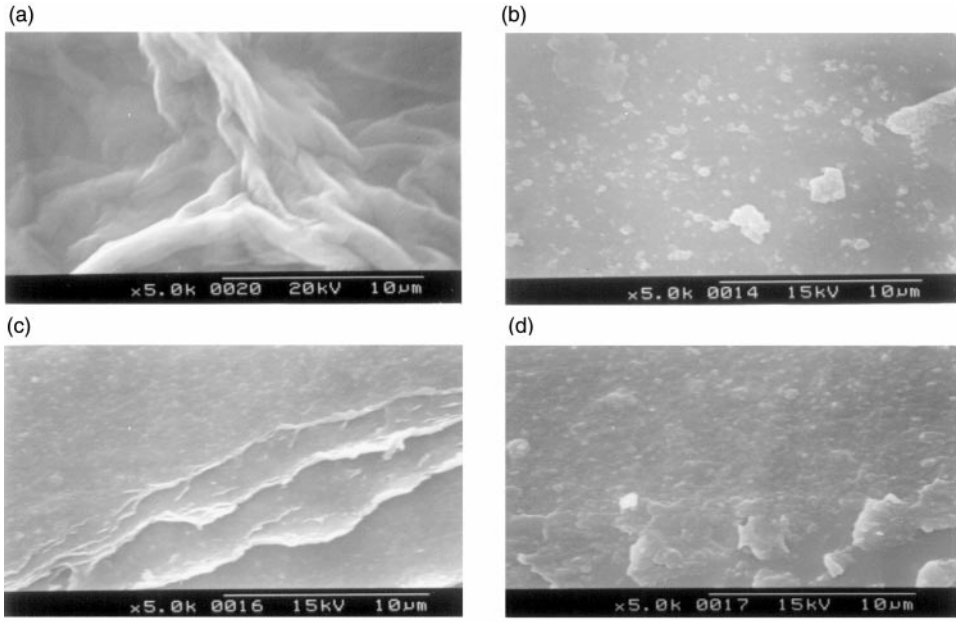


**Fig. 5** SEM micrographs of (a) $V_2O_5$ xerogel, (b) PAPSA, (c) $(PAPSA)_{0.37}V_2O_5$ and (d) $(PAPSA)_{1.18}V_2O_5$ films.

with increasing temperature, characteristic of thermally activated behavior, due to interparticle contact resistance. This behavior has also been observed in polyaniline[13] and $V_2O_5$ xerogel[14] (Fig. 6a). The low conductivity of the PAPSA film (Fig. 6b) is due to its roughness and discontinuity. PAPSA has highly ionic characteristics and therefore, smooth and continuous films can not be made easily. The conductivity of a PAPSA pellet (Fig. 6c) is much higher than that of a PAPSA film and also showed a thermally activated behavior. The conductivity of $(PAPSA)_xV_2O_5$ is similar to that of a PAPSA pellet and much better than for a PAPSA film or $V_2O_5$, even for $x$ as small as 0.07. As mentioned above, there is an electron transfer reaction between PAPSA and $V_2O_5$ in $(PAPSA)_xV_2O_5$. The higher conductivity of $(PAPSA)_xV_2O_5$ compared to PAPSA film and $V_2O_5$ may due to reduction of the $V_2O_5$ framework. However, we found that the conductivity of $(PAPSA)_xV_2O_5$ is also higher than $Na_xV_2O_5$ produced by reduction of $V_2O_5$ with NaI. Therefore, the conductivity of $(PAPSA)_xV_2O_5$ should be due to the cooperation effect between two electric conducting materials, PAPSA and $V_2O_5$. In $(PAPSA)_xV_2O_5$, PAPSA and $V_2O_5$ have close contacts and charges can be transported *via* the polymer chains or the $V_2O_5$ framework. The mobility of the charge carriers is faster than in discontinuous PAPSA film or in $V_2O_5$, in which a layer of low conducting $H_2O$ exists in the layer galleries. The close contacts in $(PAPSA)_xV_2O_5$ would explain its better conductivity relative to PAPSA film or reduced $V_2O_5$. The $V_2O_5$ xerogel in its totally oxidized state and the reduced

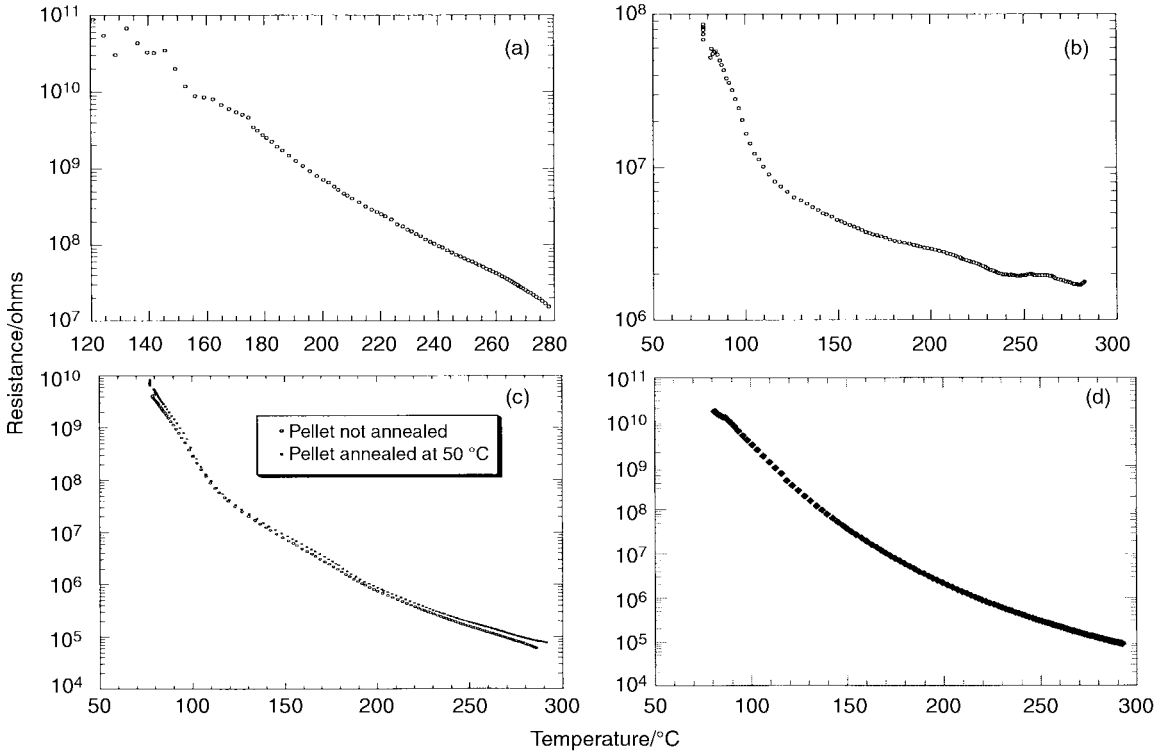


**Fig. 6** Variable temperature conductance of (a) $V_2O_5$ xerogel, (b) PAPSA film, (c) PAPSA pellet and (d) $(PAPSA)_{0.7}V_2O_5$.

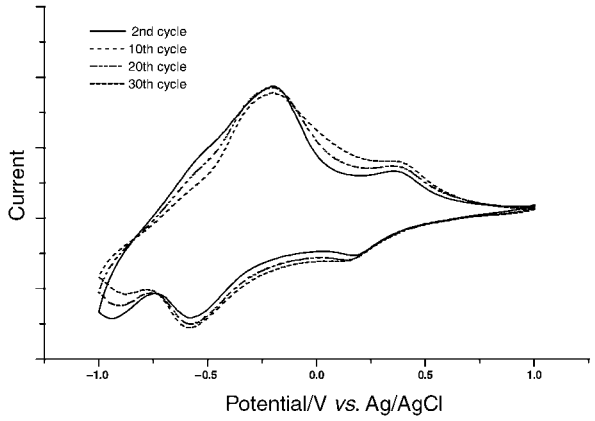


**Fig. 7** Cyclic voltammograms of $(PAPSA)_{0.7}V_2O_5$ films.

form of PAPSA are both insulating materials. On the other hand, $(PAPSA)_xV_2O_5$ are electrically conducting materials both in reduced and oxidized states: when $(PAPSA)_xV_2O_5$ nanocomposites are in the oxidized form, the PAPSA part will be in the conducting state, contrarily, when $(PAPSA)_xV_2O_5$ nanocomposites are reduced, the $V_2O_5$ part will be in the conducting state.

$V_2O_5$ xerogel is an interesting material for electrochromic devices, due to the high contrast ratio between the bleached and colored states.[15] It is well known that inorganic electrochromic materials have narrow color variation, but excellent durability, reliability and stability. On the other hand, conducting polymers show a variety of colors but generally their stability is not as good. The conducting polymer/$V_2O_5$ hybrid material may possess the advantages from both the inorganic and organic components. The combination of conducting polymers and inorganic electrochromic materials, such as $WO_3$ has been widely studied and composite based electrochromic cells had been reported.[16] We thus cast a $(PAPSA)_xV_2O_5$ thin film on a home-made ITO electrode and studied its electrochromic behavior. The cyclic voltammograms of a $(PAPSA)_{0.7}V_2O_5$ film are shown in Fig. 7. There are two reversible red-ox pairs associated with a color change from orange to greenish brown to deep green. The red-ox potentials and color variation of $(PAPSA)_xV_2O_5$ depend on the stoichiometry of the materials, as detailed in Table 3. Comparing to the redox potentials of individual components, PAPSA and $V_2O_5$, the first oxidation peak of the $(PAPSA)_xV_2O_5$ nanocomposite probably arises from the $V_2O_5$ xerogel and the second oxidation peak is the result of a cooperation effect of the polymer and $V_2O_5$ xerogel. The first reduction peak (less positive value) arises from the $V_2O_5$ xerogel and the second reduction peak, which was not observed in the $V_2O_5$ xerogel and was very weak in PAPSA, probably arises from the dispersed polymer chains (*vide infra*). This reasoning was further supported by the fact that the redox potentials of $(PAPSA)_{0.02}V_2O_5$ (with very low polymer content) are very similar to those of the $V_2O_5$ xerogel. As the polymer contents in the composites change, the potentials of both red-ox pairs also change. The potential of the first red-ox pair shows only small variation and changes irregularly, due to the different degree of interaction between PAPSA and $V_2O_5$. However, the second red-ox pair of the $(PAPSA)_xV_2O_5$ shifted to less positive values as the polymer content increased. As mentioned above, the second red-ox pair is related to the electrochemical properties of the polymer. When the PAPSA content in $(PAPSA)_xV_2O_5$ nanocomposite is increased, the distance between polymer chains decreases. Chain–chain interactions make the polymer more easily oxidized and reduced. Therefore, the red-ox potentials of the nanocomposites can be tuned from the stoichiometry of the materials. The reduction (or oxidation) of $(PAPSA)_xV_2O_5$ nanocomposites led not only to a change in color but also their transmittance of visible light. In other words, the colors and contrast ratios of the nanocomposite films can be controlled by the stoichiometry of the materials. The formation of the nanocomposites offers an excellent possibility for the synthesis of new materials with novel properties, such as electrochromism. The optical density variation and the potential application of $(PAPSA)_xV_2O_5$ nanocomposite films in electrochromic devices will be reported elsewhere. Furthermore, we found that it is difficult to make thin films from PAPSA aqueous solutions, due to its ionic character while the reduced form of $V_2O_5$ is very brittle. By contrast, thin films of $(PAPSA)_xV_2O_5$ nanocomposites are smooth and flexible in the potential range between 1.0 V and –1.0 V (*vs.* Ag/AgCl).

The electrochemical stability of the $(PAPSA)_xV_2O_5$ films was tested by red-ox cycling (Fig. 7). It was found that the oxidation peak current varied slightly in the first few cycles then steadily increased slightly up to 30 cycles. Compared to the PAPSA film, which becomes electro-inactive after 30 cycles, the electrochemical stability of $(PAPSA)_xV_2O_5$ is much better than the polymer film. Although the electrochemical stability of the $(PAPSA)_xV_2O_5$ film is not as good as the $V_2O_5$ xerogel, the mechanical properties of $(PAPSA)_xV_2O_5$ in its reduced form is better than the $V_2O_5$ xerogel, which is brittle in the highly reducing state.

**C. The structure of $(PAPSA)_xV_2O_5$ nanocomposites.** It is useful to address the driving force for the formation of conducting $(PAPSA)_xV_2O_5$ nanocomposites. There is a red-ox reaction between PAPSA and $V_2O_5$, as observed in the *in situ* polymerization/intercalation of aniline in $V_2O_5$.[3] However, the degree of reduction of $V_2O_5$ is very low since the composite is totally soluble in water (the reduced $V_2O_5$ is not soluble in water). Laser scattering particle size analysis showed that the particle size of the $(PAPSA)_xV_2O_5$ in aqueous solution is similar to that of PAPSA and $V_2O_5$. This result also indicated that there is no strong interaction between PAPSA and $V_2O_5$ after they are mixed. As mentioned previously, the *d*-spacing of water-soluble $(PAPSA)_xV_2O_5$ is $11.5 \pm 0.5$ Å and the *d*-spacing of $V_2O_5$ xerogel measured in ambient atmosphere is *ca.* 13.8 Å (due to extremely high humidity in Taiwan, water penetrated into the layer gallery of the $V_2O_5$). The lower *d*-spacing of $(PAPSA)_xV_2O_5$, compared to $V_2O_5$ suggested that the PAPSA chains block the pores of the $V_2O_5$ xerogel, preventing water penetration into the layer space of $(PAPSA)_xV_2O_5$. This proposal was further supported by TGA results, which showed that the water content of $(PAPSA)_xV_2O_5$ is less than

**Table 3** Redox potentials (*vs.* Ag/AgCl) and the corresponding color changes for $(PAPSA)_xV_2O_5$

| Materials | $E_1$(ox)/ V | Color change | $E_2$(ox)/ V | Color change | $E_2$(red)/ V | Color change | $E_1$(red)/ V | Color change |
|---|---|---|---|---|---|---|---|---|
| $V_2O_5$ xerogel | −0.15 | Deep-green to pale-green | | Pale-green to orange | | | −0.60 | Orange to deep-green |
| PAPSA | 0.0 | Green | 0.5 | Green to purple | 0.25 | Purple to green | −0.4 | Green |
| $(PAPSA)_{0.05}V_2O_5$ | −0.05 | Yellow-green to brown | 0.75 | Brown to orange | 0.41 | Orange to brown | −0.5 | Brown to yellow-green |
| $(PAPSA)_{0.7}V_2O_5$ | −0.2 | Deep-green to orange | 0.3 | Orange | 0.15 | Pale-orange to brown | −0.5 | Brown to deep-green |
| $(PAPSA)_{1.2}V_2O_5$ | −0.1 | Deep green to brown | 0.2 | Brown to purple | 0.1 | Purple to brown | −0.6 | Brown to deep-green |

[a]Scan cycle from 1.0 V to –1.0 V then back to 1.0 V.

that of $V_2O_5$ the xerogel. Therefore, the structure of $(PAPSA)_xV_2O_5$ can be described in terms of polyaniline chains confined in between two oxygen atoms of the $V_2O_5$ slabs. In general, the framework of the host becames disordered when guest molecules are inserted. Nevertheless, the crystallinity of $(PAPSA)_xV_2O_5$ nanocomposites is similar to that of $V_2O_5$ xerogel when $x$ is less than 1.0 (see Table 2). However, when $x$ is greater than 1.0, the $d$ spacing increased along with a loss of crystallinity, with the sample becoming amorphous when $x > 1.5$.

## Conclusions

This article reports the blending of an aqueous solution of organic and inorganic compounds into conducting nanocomposites. The benefits accrued by having nanoscale materials interacting with a second phase can be seen from the charge transport and the versatile electrochromic properties. The significant surface interaction between two electroactive components results in new properties on the macroscopic scale which are not observed from the individual components. This study also provides useful information, which may be of valuable help in designing new electric or electrochromic materials with specific tailor-made properties.

## Acknowledgements

The kind financial support from the National Science Council of the Republic of China (NCS 89-2113-M-008-007) is gratefully acknowledged. We thank Professor C. J. Liu for performing the conductivity measurements and Professor W. H. Lii for helping in the measurements of the XRD patterns.

## References

1 (*a*) *Better Ceramics Through Chemistry VI*, *Mater. Res. Soc. Symp. Proc*., ed. A. K. Cheetham, C. J. Brinker, M. L. McCartney and C. Sanchez, 1994, vol. 346; (*b*) U. Schubert, N. Husing and A. Lorenz, *Chem. Mater.*, 1995, **7**, 5010.
2 P. Judeinstein and C. Sanchez, *J. Mater. Chem.*, 1996, **6**, 511.
3 M. G. Kanatzidis, C.-G. Wu, H. O. Marcy and C. R. Kannewurf, *J. Am. Chem. Soc.*, 1989, **111**, 4139.
4 M. G. Kanatzidis, C.-G. Wu, H. O. Marcy, D. C. DeGroot, C. R. Kannewurf, A. Kostikas and V. Papaefthymiou, *Adv. Mater.*, 1990, **2**, 364.
5 (*a*) P. Brandt, R. D. Fisher, E. S. Martinez and R. D. Calleja, *Angew. Chem., Int. Ed. Engl.*, 1989, **28**, 1265; (*b*) P. Enzel and T. J. Bein, *Phys. Chem.*, 1989, **93**, 6270; (*c*) J. V. Caspar, V. D. Ramamurthy and R. Corbin, *J. Am. Chem. Soc.*, 1991, **113**, 600; C.-G. Wu and T. Bein, *Science*, 1994, **266**, 1013.
6 (*a*) C.-G. Wu, D. C. DeGroot, H. O. Marcy, J. L. Schindler, C. R. Kannewurf, Y. J. Liu, W. Hirpo and M. G. Kanatzidis, *Chem. Mater.*, 1996, **8**, 1992; (*b*) H. Inoue and H. Yoneyama, *J. Electroanal. Chem.*, 1987, **233**, 291.
7 (*a*) S. Baral and P. Schoen, *Chem Mater.*, 1993, **5**, 14; (*b*) A. Firouzi, D. Kumar, L. M. Bull, T. Besier, P. Sieger, Q. Huo, S. A. Walker, J. A. Zasadzinski, C. Glinka, J. Nicol, D. Margolese, G. D. Stucky and B. F. Chmelka, *Science*, 1995, **267**, 1138.
8 M. W. Weimer, H. Chen, E. P. Giannelis and D. Y. Sogah, *J. Am. Chem. Soc.*, 1999, **121**, 1615.
9 (*a*) *Hybrid Organic–Inorganic Materials*, ed. L. L. Klein and C. Sanchez, Special Issue of *J. Sol–Gel Sci. Technol.*, 1995, **5**; (*b*) *Sol–Gel Technology for Thin Film, Fiber, Preforms, Electronics and Especialty Shapes*, ed. L. L. Klein , Noyes, Park Ridge, NJ, 1988; (*c*) H. Schmidt, in *Ultrastructure Processing of Advanced Materials*, ed. D. R. Uhlmann and D. R. Ulrich, Wiley, New York, 1992, ch. 38; (*d*) *Hybrid Organic–Inorganic Composites*, ed. J. E Mark, C. Y.-C. Lee and P. A. Bianconi, ACS Symp. Ser., Washington, DC, 1995, vol. 585.
10 M. Lira-Cant and P. Gomez-Romero, *J. Solid State Chem.*, 1999, **147**, 601.
11 (*a*) C. DeArmitt, C. P. Armes, J. Winter, F. A. Urid, J. Gottesfeld and C. Mombuerquette, *Polymer*, 1993, **34**, 158; (*b*) S.-A. Chen and G.-W. Hwang, *J. Am. Chem. Soc.*, 1995, **117**, 10055; (*c*) H. S. O. Chan, P. K. H. Ho, S. C. Ng, B. T. Tan and G. K. L. Tan, *J. Am. Chem. Soc.*, 1995, **117**, 8517; (*d*) M. T. Nguyen, P. J. Kasai, L. A. Miller and F. Diaz, *Macromolecules*, 1994, **27**, 3625.
12 J. Lemerle, L. Nejem and J. Lefebvre, *J. Inorg. Nucl. Chem.*, 1980, **42**, 17.
13 F. Zuo, M. Angelopoulos, A. G. MacDiarmid and A. J. Epstein, *Phys. Rev. B*, 1987, **36**, 3475.
14 J. Bullot, O. Gallais, M. Gauthier and J. Livage, *Appl. Phys. Lett.*, 1980, **36**, 986.
15 (*a*) A. G. MacDiarmid and W. Zheng, *MRS Bull.*, 1997, 24–19; (*b*) J. Gustafsson, O. Inganas and A. Andersson, *Synth. Met.*, 1991, **62**, 17.
16 (*a*) A. R. Rocco, M.-A. DePao, A. Zanelli and M. Mastragostine, *Electrochim. Acta*, 1996, **41**, 2805; (*b*) T. Ohtsuka, T. Wakabayashi and H. Einaga, *Synth. Met.*, 1996, **79**, 235.